Available online at www.sciencedirect.com
SCIENCE DIRECT®
International Journal of Heat and Mass Transfer 48 (2005) 3097–3106
International Journal of HEAT and MASS TRANSFER
www.elsevier.com/locate/ijhmt

Transient buoyant convection of air in an enclosure under strong magnetic effect

Seung Ho Lee [a], Jae Min Hyun [b,*]

[a] CAE Team, R&D Center, Halla Climate Control Corporation, 1689-1, Sinil-dong, Daedeok-gu, Daejeon 306-230, South Korea
[b] Department of Mechanical Engineering, Korea Advanced Institute of Science and Technology, 373-1 Kusong-dong, Yusong-gu, Daejeon 305-701, South Korea

Received 27 August 2004; received in revised form 11 February 2005
Available online 18 April 2005

Abstract

A numerical study is made of transient convective cool-down of air in a cylindrical container when both gravity and magnetizing force act. The magnetizing force is generated in an inhomogeneous magnetic field for an electrically non-conducting fluid with high magnetic susceptibility. Cooling of air is accomplished by abruptly lowering the temperature of the cylindrical sidewall under a strong vertical magnetic field. Comprehensive numerical computations are obtained for ranges of pertinent external parameters. The behavior of flow and temperature fields are delineated as the radius and axial position of the electrical coil are varied. When the magnetizing force is parallel to gravity, the flow is invigorated and cool-down process is facilitated. When the magnetizing force opposes the gravity, the overall cool-down process is least effective when the strength of magnetizing force is comparable to gravity.

1. Introduction

The magnetic effect on fluid transport phenomena has been extensively studied over the decades. The majority of these investigations, however, have dealt with the fluid motions associated with the Lorentz force. A substantial body of knowledge has been accumulated on this account, and industrial applications have been noteworthy. It is important to point out that the Lorentz force effect is brought forth only for electrically conducting fluids.

A new and different class of magnetic effect on fluid flow, in the form of magnetizing force, has received attention recently. As emphasized in Refs. [1–10], the magnetizing force is induced in ordinary fluids when the gradients of the magnetic field exist. This force is expressed as the product of the gradient of the square of magnetic induction and the magnetic susceptibility of the working fluid. The significance of this magnetizing force has long been recognized. However, in order for this force to be of practical relevance, it is required that very strong magnetic fields should be applied. In the past, producing very strong magnetic fields was impracticable. Therefore, in a magnetic field of modest strength, the role of the magnetizing force was not notable, and, accordingly, utilization of the magnetizing force was not actively pursued.

The advent of a superconducting magnet opened the way for serious evaluations of the magnetizing force as well as engineering applications to control the fluid transport processes. It is stressed that, unlike the

* Corresponding author. Tel.: +82 42 869 3012; fax: +82 42 869 3210.
E-mail address: jmhyun@cais.kaist.ac.kr (J.M. Hyun).

0017-9310/$ - see front matter © 2005 Elsevier Ltd. All rights reserved.
doi:10.1016/j.ijheatmasstransfer.2005.02.017

Nomenclature

$\vec{a}$	position vector (r_c, z_c) [m]
$\vec{A}$	$\vec{a}/x_a = (R_c, Z_c)$
$\vec{b}$	magnetic induction [T]
b_a	reference magnetic induction, $\mu_m i/h$ [T]
$\vec{B}$	dimensionless magnetic induction, $\vec{b}/b_a$
d	diameter of the cylinder [m]
d_c	diameter of coil [m]
$\vec{f}$	magnetizing force [N/m^3]
h	height of the cylinder [m]
i	electric current [A]
p	pressure [Pa]
p_a	reference pressure, $\rho\kappa^2/h^2$ [Pa]
p'	perturbed pressure [Pa]
P	dimensionless pressure, p'/p_a
Pr	Prandtl number, ν/κ
r	radial coordinate [m]
r_c	radius of coil [m]
r_0	radius of cylinder [m]
$\vec{r}$	position vector in the cylinder (r, z) [m]
$\vec{R}$	$\vec{r}/x_a = (R, Z)$
Ra	Rayleigh number, $g\beta\Delta T h^3/(\kappa\nu)$
t	time [s]
t_a	h^2/κ [s]
T	temperature [K]
T_0	reference temperature [K]
u	velocity in the radial direction [m/s]
u_a	κ/h [m/s]
U	dimensionless velocity in the radial direction, u/u_a
w	velocity in the axial direction [m/s]
w_a	κ/h [m/s]
W	dimensionless velocity in the axial direction, w/w_a
x_a	reference length [m]
z	axial coordinate [m]
z_c	axial position of coil [m]

Greek symbols

β	volumetric expansion coefficient [K^{-1}]
γ	$\chi b_a^2 \xi/(\mu_m g h)$
κ	thermal diffusivity [m/s^2]
μ	viscosity [Pa s]
μ_m	magnetic permeability [H/m]
ν	kinetic viscosity [m^2/s]
ρ	density [kg/m^3]
θ	dimensionless temperature $(T - T_0)/\Delta T$
τ	dimensionless time, t/t_a
ξ_{O_2}	molar fraction of oxygen gas
χ_{O_2}	magnetic susceptibility of oxygen gas [m^3/kg]

Subscripts

a	reference value
c	coil
m	magnetic effect
w	sidewall
0	reference state
O_2	oxygen gas

Lorentz force, the magnetizing force arises in both electrically conducting and electrically non-conducting fluids.

Several of the fundamental convective flow and heat transfer models, under the influence of magnetizing force, have been documented in the pioneering treatises, e.g., Refs. [3–7]. The flow characteristics with varying magnetic susceptibility were probed, and comparisons were made between the experimental and numerical results. Wakayama [1,2] demonstrated that, by means of the magnetizing force, an effective control of steady-state convective flow is feasible. The analogous roles played by the gravity force and magnetizing force were discussed in these prior publications.

In the present paper, the possibility of controlling the time-dependent transient process of a fluid by deploying the magnetizing force is examined. Specifically, the cooling process of initially hot air in an enclosed cylinder is scrutinized. When there is no magnetic effect, the cool-down of air is governed by the conventional gravity-caused buoyant convection. However, by passing electric current in the coil surrounding the cylindrical container, the effect of magnetizing force is activated, and the fluid flow is altered. Modifications to the usual transient buoyant convection by applying strong magnetic fields are described in the present undertaking. Numerical computations are performed, and the calculated results illustrate that substantial alterations to the flow and heat transfer of air are observed. These numerical exercises indicate that the magnetizing force effect can be a major element to accomplish an efficient control of transient transport processes. The time-dependent evolutions of fluid motions and attendant heat transfer are depicted by analyzing the computational results. The effects of external parameters are scrutinized, and the practical utility of magnetic flow control is discussed.

2. Formulation and numerical model

Consider a vertically mounted cylinder [radius r_0 and height h, with aspect ratio $(Ar(\equiv h/r_0) = 1.0)$], which is filled with air at temperature T_0. The cylinder is located inside a concentric coil, and by passing electrical current

in the coil, a magnetic field is created in the cylinder. The top and bottom endwalls of the cylinder are thermally insulated. In the initial state, the temperature of the cylinder sidewall is impulsively set at T_w, which is lower than $T_0[\Delta T \equiv T_0 - T_w]$. Consequently, cool-down of the air proceeds under the influence of both the gravity and the magnetizing force, and this constitutes the task of the present endeavor.

As stipulated in [1–7], the magnetizing force for air, $\vec{f}_m$, is expressed as

$$\vec{f}_m = \frac{1}{2\mu_m}\rho\chi\xi\nabla b^2 \tag{1}$$

in which μ_m denotes the magnetic permeability, ρ density, χ magnetic susceptibility, ξ molar fraction, and b the magnitude of $\vec{b}$, the magnetic induction vector. Basically, in the ensuing development, the governing Navier–Stokes equations are formulated to include the above magnetizing force as an additional body force term. In the present development, axisymmetry is assumed.

The complete time-dependent basic equations consist of the continuity equation, energy equation, the momentum equations and the equation for Biot–Savart's law. The detailed derivations of the pertinent equations and the background rationale have been elaborated in prior publications [3–7]. The properly non-dimensionalized governing equations are [the symbols are defined in the nomenclature]:

$$\nabla\cdot\vec{U} = 0, \tag{2}$$

$$\frac{D\theta}{D\tau} = \nabla^2\theta, \tag{3}$$

$$\frac{D\vec{U}}{D\tau} = -\nabla P + Pr\nabla^2\vec{U} + Ra\ Pr\theta\left[-\gamma\nabla B^2 + \begin{pmatrix}0\\0\\1\end{pmatrix}\right], \tag{4}$$

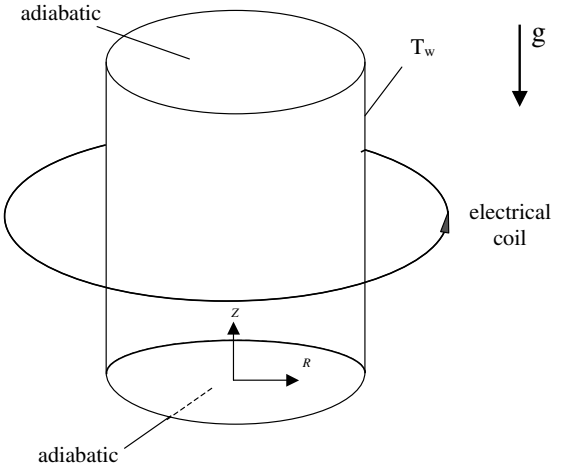

Fig. 1. Schematic of the system.

$$\vec{B} = \frac{1}{4\pi}\oint\frac{(\vec{A}-\vec{R})\times d\vec{A}}{|\vec{A}-\vec{R}|^3} \tag{5}$$

in which non-dimensionalization was implemented as

$$R = \frac{r}{h},\quad Z = \frac{z}{h},\quad R_c = \frac{r_c}{h},\quad Z_c = \frac{z_c}{h},$$

$$U = \frac{uh}{\kappa},\quad W = \frac{wh}{\kappa},\quad \tau = \frac{t}{(h^2/\kappa)},\quad P = \frac{P'}{P_a},$$

$$\theta = \frac{T-T_0}{(T_0-T_w)},\quad \vec{B} = \frac{\vec{b}}{b_a},\quad P_a = \frac{\rho\kappa^2}{h^2},\quad b_a = \frac{\mu_m i}{h},$$

$$Pr = \frac{\nu}{\kappa},\quad Ra = \frac{g\beta(T_0-T_w)h^3}{\kappa},$$

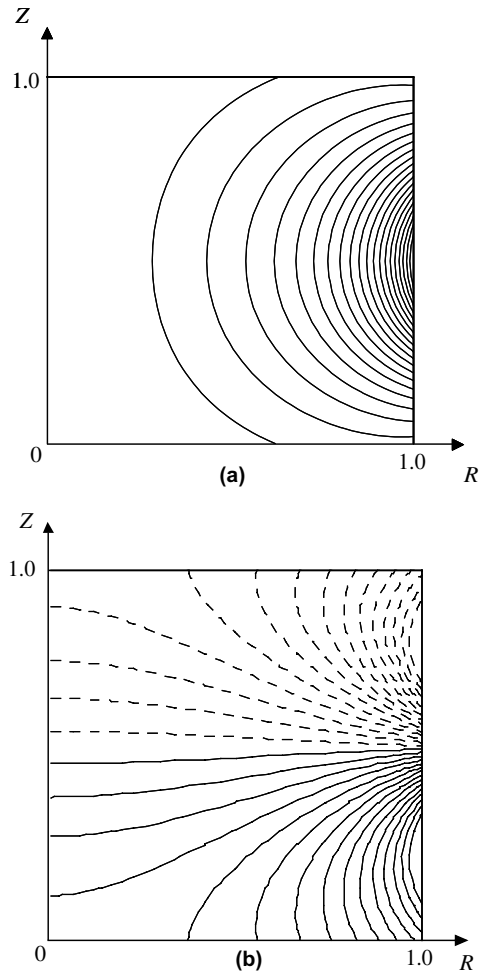

Fig. 2. Contour plots of ∇B^2. $R_c = 1.5$, $Z_c = 0.5$, $\gamma Ra = 10^7$. (a) $\frac{\partial(B^2)}{\partial R}: \left(\frac{\partial(B^2)}{\partial R}\right)_{max} = 6.61\times10^{-1}$, $\left(\frac{\partial(B^2)}{\partial R}\right)_{min} = 4.41\times10^{-2}$, contour increment $= 3.25\times10^{-2}$; (b) $\frac{\partial(B^2)}{\partial Z}: \left(\frac{\partial(B^2)}{\partial Z}\right)_{max} = 3.67\times10^{-1}$, $\left(\frac{\partial(B^2)}{\partial Z}\right)_{min} = -3.67\times10^{-1}$, contour increment $= 2.53\times10^{-2}$.

$$\gamma \equiv \frac{\chi_O b_a \xi}{\mu_m g h}.$$

In Eq. (5), $\vec{A}$ denotes the non-dimensional axisymmetric position vector (R_c, Z_c) of an infinitesimal element of the electrical coil $d\vec{A}$, and $\vec{R}$ is the position vector of the interior point in the cylinder. In the non-dimensionalized basic equations, the relevant non-dimensional parameters are the Prandtl number Pr, Rayleigh number Ra, which are familiar in the buoyant convection problems. In the present work, the magnitude of magnetizing force is represented by γ, which is a measure of the relative importance of the magnetizing force effect and the conventional gravity effect. As is evident in Eq. (5), for the positions inside the cylinder, $\vec{B}$ is determined by the location and geometry of the electrical coil. Consequently, as can be seen in the last two terms in Eq. (4), the magnetizing force, which is proportional to ∇B^2, is not spatially uniform, whereas the gravitational acceleration is constant.

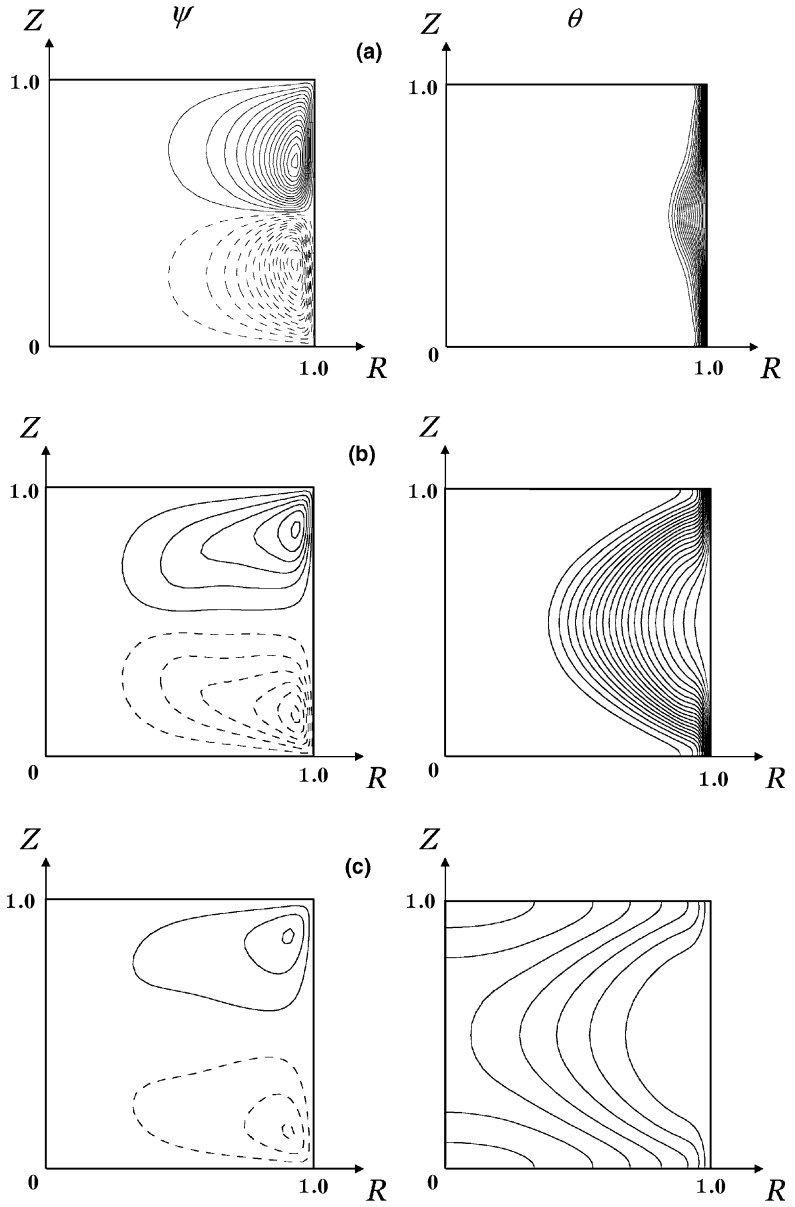

Fig. 3. Sequential plots of stream functions ψ and isotherms θ. $R_c = 1.5$, $Z_c = 0.5$, $\gamma Ra = 10^7$, and $Pr = 0.7$. (a) $\tau = 0.001$; (b) $\tau = 0.01$; (c) $\tau = 0.1$. Stream functions (ψ): $\psi_{max} = 1.64 \times 10$, $\psi_{min} = -1.64 \times 10$, $\Delta\psi = 1.13$. Isotherms (θ): $\theta_{max} = -6.23 \times 10^{-2}$, $\theta_{min} = -9.37 \times 10^{-1}$, $\Delta\theta = 4.61 \times 10^{-2}$.

The initial conditions are stated:

$$U = W = 0, \quad \theta = 0 \quad \text{at } \tau < 0$$

and the boundary conditions are written as

$$U = W = 0, \quad \frac{\partial \theta}{\partial Z} = 0 \quad \text{at } Z = 0, 1,$$

$$U = 0, \quad \frac{\partial W}{\partial R} = \frac{\partial \theta}{\partial R} = 0 \quad \text{as } R \to 0,$$

$$U = W = 0, \quad \theta = -1 \quad \text{at } R = 1.$$

The numerical procedures adopted here are the finite volume method based on the well-established SIMPLEC algorithm [11]. The discretizations followed the QUICK scheme [12,13]. For most calculations, a (40×40) grid network in the $(R$–$Z)$ plane was used. Grid clustering was made in order to place more grid points near the cylinder walls where steep flow gradients are anticipated. At each iteration level, convergence was declared when the maximum relative changes in flow variables fell below 10^{-4}. The verification of the numerical model was carried out by systematically repeating the unsteady buoyant convection problems as well as the steady flow under magnetizing force. The computed results demonstrated broad agreement with the published data. The purpose of this study is not to develop or refine the computational techniques. No claims are made as to the newness or innovativeness of the numerical methods. The objective of this study is to unveil and explain the physical features of the transient process. Therefore, well-documented numerical schemes were utilized, and computations were performed in a routine manner.

3. Results and discussion

As specific examples, comprehensive numerical computations were carried out for a cylinder of aspect ratio $Ar = 1.0$, $Ra = 10^7$ and $Pr = 0.71$. In order to concentrate on the effect of the magnetizing force, the significant external parameters are the strength of the magnetic induction and the radius and position of the electrical coil. The modern superconducting magnets [3–5] produce a magnetic field up to 10 T; therefore, the range of the parameter γ was set $\gamma = 1.0$–30.0. In view of a practicable system, the radius of coil was set $R_c = 1.1$–4.0, and the vertical location of the coil was within the height of the cylinder $Z_c = 0.0$–1.0 (Fig. 1). These parameters were selected such that the system will be practical and relevant to the experimental situations [3–7].

3.1. Case when only the magnetizing force is present

First, a series of computations were made for the cases when there is no gravity force. This portrays the cool-down process under the influence of magnetizing force only. In order to acquire a rudimentary understanding of the magnetizing force, typical patterns of the (R- and Z-) components of the vector ∇B^2, i.e., $\frac{\partial(B^2)}{\partial R}$ and $\frac{\partial(B^2)}{\partial Z}$, are exemplified in Fig. 2 when the coil is located at the mid-height of the cylinder, $Z_c = 0.5$. Expectedly, ∇B^2 is large near the cylindrical wall. The top and bottom endwall disks ($Z = 0.0$ and $Z = 1.0$) are thermally insulated; thus, when the temperature of the cylindrical wall is lower then the interior air, much of the density gradient $\nabla\rho$ points radially outward. As

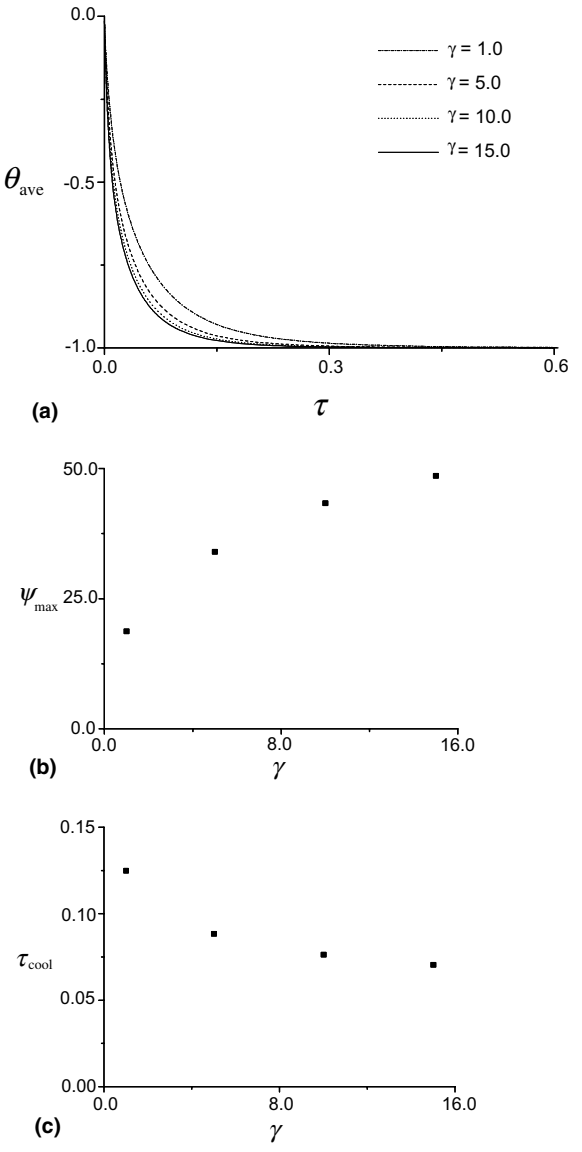

Fig. 4. Effects of the magnitude of magnetizing force (γRa). $R_c = 1.5$, $Z_c = 0.5$, $Ra = 10^7$, and $Pr = 0.7$: (a) average temperature (θ_{ave}), (b) maximum value of stream function (ψ_{max}), (c) cooling-time (τ_{cool}).

shown in Fig. 2(a), $\frac{\partial(B^2)}{\partial R}$ and $\nabla\rho$ are largely parallel near the wall region of the cylinder. Consequently, the contribution of $\frac{\partial(B^2)}{\partial R}$ to the fluid flow is comparatively minor. On the other hand, $\frac{\partial(B^2)}{\partial Z}$ entails considerable z-variations, especially in the mid-height region, as illustrated in Fig. 2(b). This points to the relative importance of $\frac{\partial(B^2)}{\partial Z}$ in the make-up of the magnetizing force.

The sequential pictures of cool-down process of air by the workings of magnetizing force are displayed in Fig. 3. The meridional flows are represented by the stream function ψ, where $U = \frac{1}{r}\frac{\partial\psi}{\partial z}$, $W = -\frac{1}{r}\frac{\partial\psi}{\partial r}$. At early times, strong flows are generated close to the cylindrical wall. These consist of a clockwise (anti-clockwise) circulation in the upper (lower) portion of the cylinder. The temperature field indicates that heat transfer proceeds faster near the level of the coil. As time elapses, the temperature difference between the cylindrical wall and the interior fluid is reduced. It is noted that the magnetic susceptibility of air is a function of temperature. Therefore, at later times, the fluid motions are attenuated, and the global heat transport relies more on conduction.

The quantitative data on the effect of the strength of magnetic induction on the overall cool-down process are presented in Fig. 4. As stated previously, the strength of magnetic effect is gauged by the parameter γ [3–5]. Computations are made as γ varies, while the other parameters are fixed. Fig. 4(a) exhibits the evolution of the average bulk temperature θ_{ave} of air. In the present calculations, θ_{ave} for air inside the cylinder is defined as

$$\theta_{ave}(\tau) = \frac{\int_0^h \int_0^a \int_0^{2\pi} \theta R \, d\phi \, dR \, dZ}{\pi a^2 h}. \tag{6}$$

Clearly, as γ increases, θ_{ave} decreases at a faster rate. This indicates that the overall cool-down process proceeds more efficiently as the fluid is subjected to a stronger magnetic field. Similarly, the variation of the maximum value of stream function, ψ_{max}, versus γ is shown in Fig. 4(b). This demonstrates that the flow is invigorated as γ increases. Also, the cooling time, which is the time duration for θ_{ave} to reach 90% of the wall

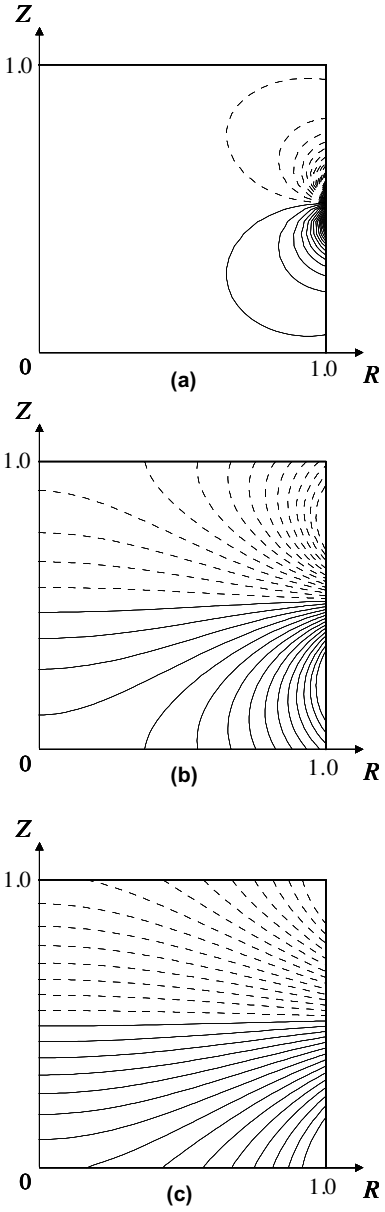

Fig. 5. Contour plots of $\frac{\partial(B^2)}{\partial Z}$. $Z_c = 0.5$, $\gamma Ra = 10^7$. (a) $R_c = 1.1$: $\left(\frac{\partial(B^2)}{\partial Z}\right)_{max} = 2.11 \times 10$, $\left(\frac{\partial(B^2)}{\partial Z}\right)_{min} = -2.11 \times 10$, contour increment = 1.45; (b) $R_c = 1.5$: $\left(\frac{\partial(B^2)}{\partial Z}\right)_{max} = 3.67 \times 10^{-1}$, $\left(\frac{\partial(B^2)}{\partial Z}\right)_{min} = -3.67 \times 10^{-1}$, contour increment = 2.53×10^{-2}; (c) $R_c = 2.0$: $\left(\frac{\partial(B^2)}{\partial Z}\right)_{max} = 7.24 \times 10^{-2}$, $\left(\frac{\partial(B^2)}{\partial Z}\right)_{min} = -7.24 \times 10^{-2}$, contour increment = 4.99×10^{-3}.

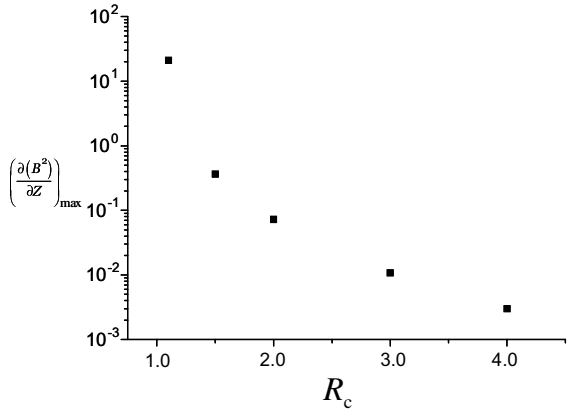

Fig. 6. Plots of the maximum $\frac{\partial(B^2)}{\partial Z}$ versus the radius of coil (R_c). $Z_c = 0.5$, $\gamma Ra = 10^7$.

temperature, τ_{cool}, versus γ is plotted in Fig. 4(c). These computed results are indicative of the effectiveness of the magnetizing force in accomplishing the cool-down process of air.

Next, computations were made by varying the radius (R_c) and the vertical location (Z_c) of the electrical coil. The distributions of $\frac{\partial(B^2)}{\partial Z}$ with different values of R_c are depicted in Fig. 5. It is clear that when R_c is small, $\frac{\partial(B^2)}{\partial Z}$ is large in the region close to the cylindrical wall. As R_c increases, the resulting distributions of $\frac{\partial(B^2)}{\partial Z}$ are more uniform in much of the cylinder interior. In Fig. 6, the change in the maximum value of $\frac{\partial(B^2)}{\partial Z}$ versus R_c is shown. As can be inferred in the Biot–Savart's law,

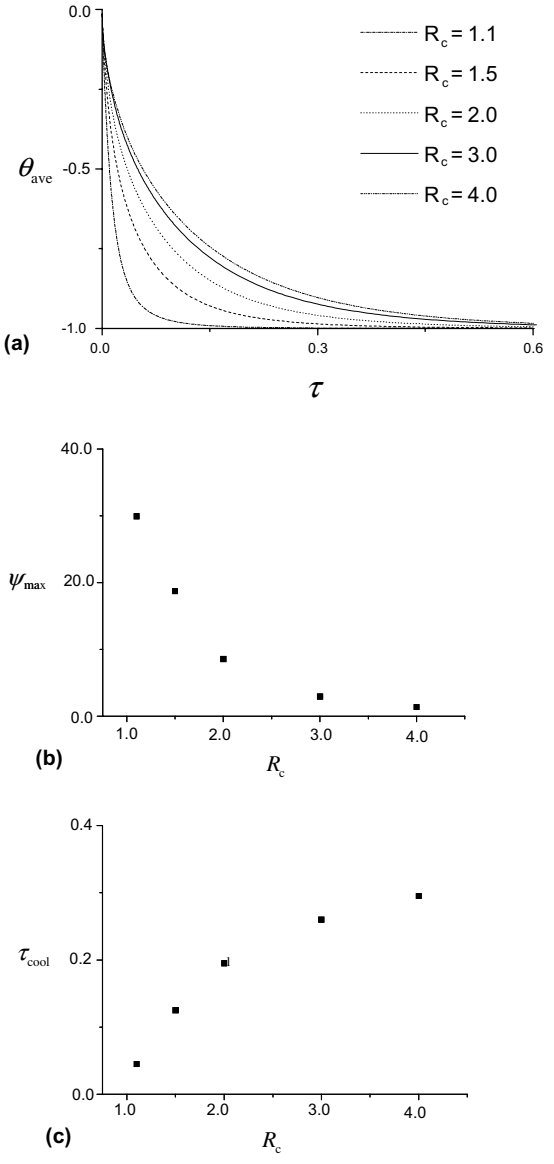

Fig. 7. Effects of the radius of coil (R_c). $Z_c = 0.5$, $\gamma Ra = 10^7$, and $Pr = 0.7$: (a) average temperature (θ_{ave}), (b) maximum value of stream function (ψ_{max}), (c) cooling-time (τ_{cool}).

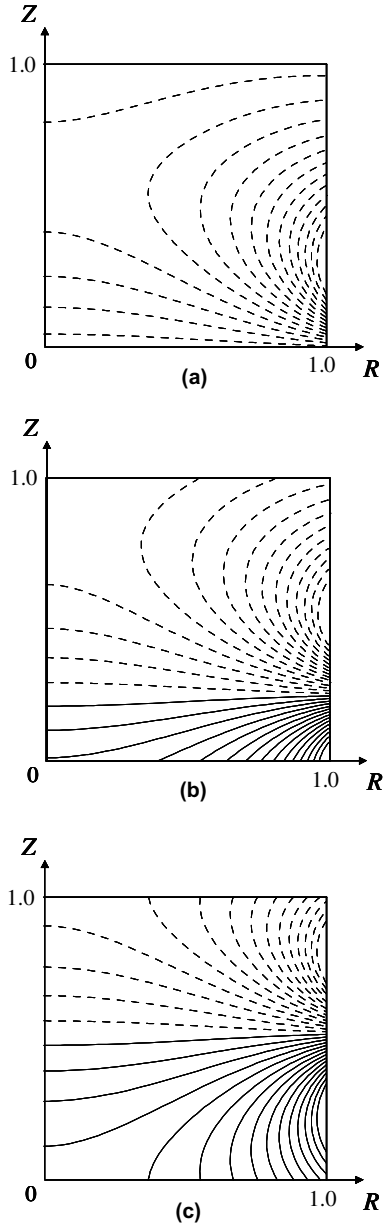

Fig. 8. Contour plots of $\frac{\partial(B^2)}{\partial Z}$. $R_c = 1.5$, $\gamma Ra = 10^7$. (a) $Z_c = 0.0$: $\left(\frac{\partial(B^2)}{\partial Z}\right)_{max} = -2.67 \times 10^{-2}$, $\left(\frac{\partial(B^2)}{\partial Z}\right)_{min} = -3.67 \times 10^{-1}$, contour increment = 2.53×10^{-2}; (b) $Z_c = 0.25$: $\left(\frac{\partial(B^2)}{\partial Z}\right)_{max} = 3.65 \times 10^{-1}$, $\left(\frac{\partial(B^2)}{\partial Z}\right)_{min} = -3.67 \times 10^{-1}$, contour increment = 2.53×10^{-2}; (c) $Z_c = 0.5$: $\left(\frac{\partial(B^2)}{\partial Z}\right)_{max} = 3.67 \times 10^{-1}$, $\left(\frac{\partial(B^2)}{\partial Z}\right)_{min} = -3.67 \times 10^{-1}$, contour increment = 2.53×10^{-2}.

the magnetic field $\vec{B}$ is inversely proportional to the square of distance. Consequently, the decrease of $\frac{\partial(B^2)}{\partial Z}$ is notable even when the radius of coil R_c increases moderately.

The impact of R_c on the overall cool-down process is exhibited in Fig. 7. As R_c increases, the flow is less invigorated, as shown by the decrease of ψ_{max}, and the cool-down time τ_{cool} increases, which indicates the weakening magnetizing force.

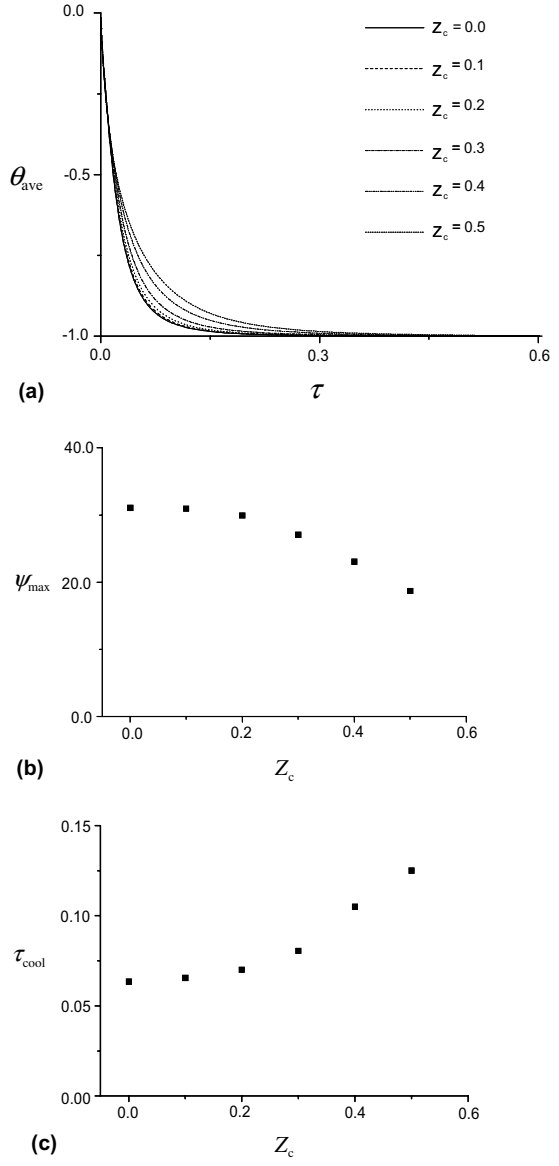

Fig. 9. Effects of the vertical location of coil (Z_c). $R_c = 1.5$, $\gamma Ra = 10^7$, and $Pr = 0.7$: (a) average temperature (θ_{ave}), (b) maximum value of stream function (ψ_{max}), (c) cooling-time (τ_{cool}).

The effect of the vertical location Z_c of coil is scrutinized in Fig. 8, which displays the distributions of $\frac{\partial(B^2)}{\partial Z}$. When the coil is located at the same level as the bottom endwall of the cylinder, $Z_c = 0.0$, $\frac{\partial(B^2)}{\partial Z}$ is negative throughout the cylinder interior. Therefore, the flow generated constitutes a single clockwise-circulating cell in the entire cylinder. In the case of Fig. 8(b), the vertical location of the coil is between the bottom endwall and the cylinder mid-height. Therefore, $\frac{\partial(B^2)}{\partial Z}$ is negative (positive) in the larger (smaller) upper (lower) part of the cylinder, which produces a clockwise (counter-clockwise) circulating cell in that region. As illustrated in Fig. 9, the transient process is facilitated when the vertical location of the coil is near the bottom (or top) endwall, i.e., $Z_c = 0.0$ (or 1.0). The magnetic effect is least effective when the vertical location of the coil is at the mid-height of the cylinder ($Z_c = 0.5$). As stipulated earlier, when $Z_c = 0.0$, the entire cylinder is occupied by a large clockwise-circulating cell. This is effective in bringing about fluid motions and transport processes. On the other hand, when $Z_c = 0.5$, two smaller-sized cells, each circulating in the opposite directions, are generated. These two cells interfere with each other in effectuating transport processes. In this case, accordingly, ψ_{max} decreases and τ_{cool} increases. This implies that the magnetizing

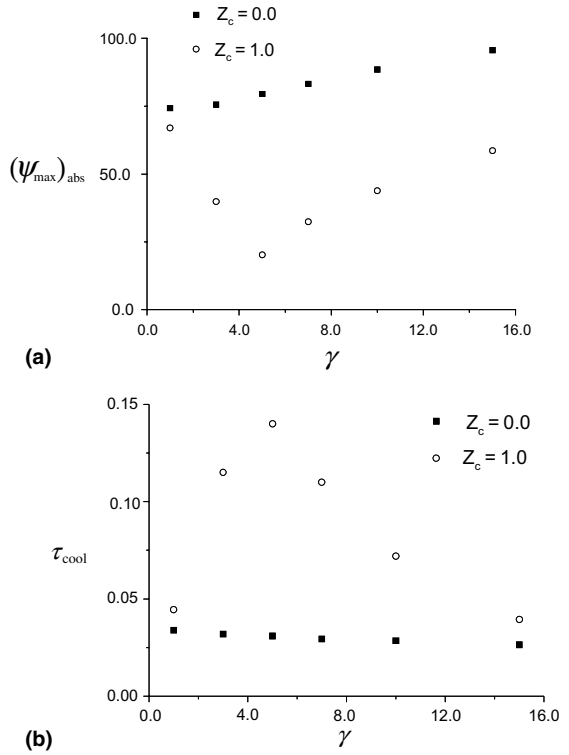

Fig. 10. Effects of the vertical location of coil (Z_c): $Z_c = 0.0$ and $Z_c = 1.0$ for $(\psi_{max})_{abs}$ and τ_{cool}; $R_c = 1.5$, $Ra = 10^7$, and $Pr = 0.7$. (a) $(\psi_{max})_{abs}$; (b) τ_{cool}.

force is least effective in accomplishing the cool-down process.

3.2. Case when both gravity and magnetizing force are present

Now, consider the cases when both the gravity and the magnetic effect exist so that fluid motions arise by both the conventional buoyancy-driven convection [14–17] and the magnetizing force.

3.2.1. When gravity and magnetizing force are in the same direction

As remarked earlier, when the electrical coil is located at the level of the bottom endwall ($Z_c = 0.0$), $\frac{\partial(B^2)}{\partial Z}$ is negative in the entire cylinder. Thus, the magnetizing force acts in the same direction as gravity. However, it should be mentioned that, unlike gravity, which is spatially uniform, $\frac{\partial(B^2)}{\partial Z}$ is spatially non-uniform. In this case, the above two forces are cooperative. Therefore, as the magnetic effect increases, the flow intensifies, i.e., $(\psi_{max})_{abs}$ increases, and the cool-down time shortens, which is illustrated in Fig. 10.

3.2.2. When gravity and magnetizing force are in the opposite direction

When the electrical coil is located at the level of the top endwall ($Z_c = 1.0$), the magnetizing force and gravity act in the opposite directions. Inspection of the results for $Z_c = 1.0$ in Fig. 10 reveals that $(\psi_{max})_{abs}$ takes the lowest value[and τ_{cool} takes the largest value] when γ takes a value around $\gamma_m \cong 4.5$. Clearly, when γ is small ($\gamma < \gamma_m$), the gravity outweighs the magnetic effect. As γ increases in the regime $\gamma < \gamma_m$, the counteracting effect of

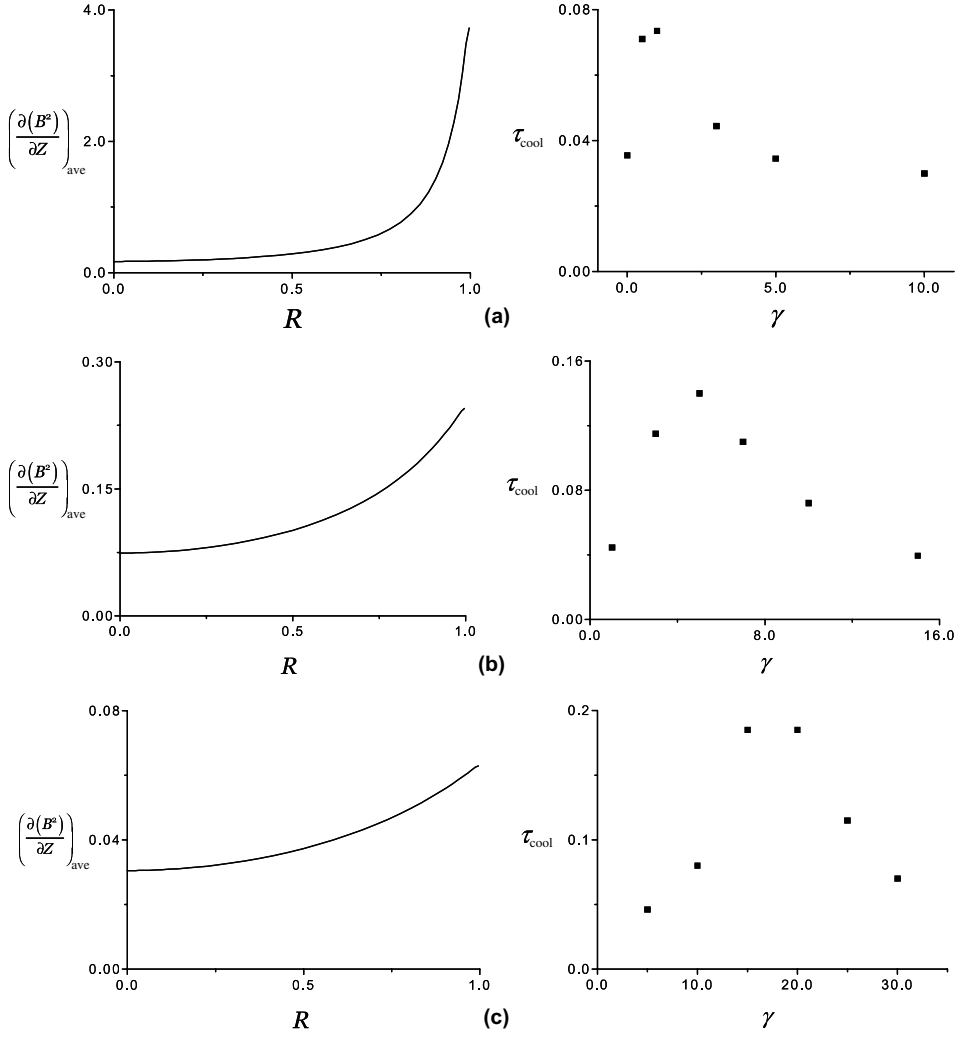

Fig. 11. Effects of the radius of coil (R_c) for τ_{cool}. $Z_c = 1.0$, $Ra = 10^7$, and $Pr = 0.7$. (a) $R_c = 1.1$; (b) $R_c = 1.5$; (c) $R_c = 2.0$.

magnetizing force increases. Therefore, in this parameter range, by increasing the magnetic strength, the flow development is further suppressed, and it takes longer time to cool-down to the final state. On the other hand, when γ is large, i.e., $\gamma > \gamma_m$, the magnetic effect dominates, and the flow intensifies as γ increases, which is shown in increasing $(\psi_{max})_{abs}$ and in decreasing τ_{cool}. It is summarized that the suppression of overall convective heat transfer can be achieved by noting carefully that the gravity and magnetizing force are opposing.

The influence of the coil radius R_c is illustrated in Fig. 11, with $Z_c = 1.0$. First, it is discernible that the strength of magnetizing force, represented by $\frac{\partial(B^2)}{\partial Z}$, decreases rapidly as R_c increases moderately (compare the units for $\left(\frac{\partial(B^2)}{\partial Z}\right)_{ave}$ in Fig. 11. Here, $\left(\frac{\partial(B^2)}{\partial Z}\right)_{ave}$ indicates the vertically averaged value of $\frac{\partial(B^2)}{\partial Z}$). Also, the R-distribution of $\frac{\partial(B^2)}{\partial Z}$ becomes steeper as the coil shrinks in size. The behavior of τ_{cool} with γ should also be noted. For this purpose, it is recalled that the total body forces in the equation are expressed as $[-\gamma\nabla B^2 + \hat{e}_z]$, where $\hat{e}_z$ is the unit vector in the vertical direction. In the opposing case, therefore, the effect of the magnetizing force and gravity are comparable when $\gamma\nabla B^2$ takes a value close to unity. An interrogation of the plots of $\frac{\partial(B^2)}{\partial Z}$ as well as the values of γ_m leads to the conclusion that the suppression of convective flow is most effective when the parameter $\gamma_m \frac{\partial(B^2)}{\partial Z}$ is close to unity.

4. Conclusion

When the system is under the influence of magnetic effect only, the magnetizing force increases as the magnetic susceptibility and $\frac{\partial(B^2)}{\partial Z}$ increase. The fluid motion intensifies as γ increases. The impact of the coil radius R_c is significant, as the transport process is invigorated as R_c decreases. The flow intensifies when the coil is located closer to the endwalls of the cylinder. In this case, a large single cell occupies the cylinder interior, and the overall convective heat transfer is facilitated.

When both the magnetizing force and gravity are present, the vertical position of coil Z_c is a crucial parameter. When $Z_c = 0.0$, both forces are cooperating to promote the convective process. When $Z_c = 1.0$, the two forces are counteracting. The heat transfer characteristics are divided into two parameter regimes, $\gamma < \gamma_m$ and $\gamma > \gamma_m$. The most effective suppression of overall heat transfer can be achieved in this system when γ is close to γ_m.

Acknowledgment

This work was supported by Korean Research Foundation Grant [KRF-2003-041-D00129].

References

[1] B. Bai, A. Yabe, J. Qi, N.I. Wakayama, Quantitative analysis of air convection caused by magnetic-fluid coupling, AIAA J. 37 (1999) 1538–1543.
[2] J. Qi, N.I. Wakayama, A. Yabe, Magnetic control of thermal convection in electrically non-conducting or low-conducting paramagnetic fluids, Int. J. Heat Mass Transfer 44 (2001) 3043–3052.
[3] T. Tagawa, H. Ozoe, K. Inoue, M. Ito, K. Sassa, S. Asai, Transient characteristics of convection and diffusion of oxygen gas in an open vertical cylinder under magnetizing and gravitational forces, Chem. Eng. Sci. 56 (2001) 4217–4223.
[4] T. Tagawa, R. Shigemitsu, H. Ozoe, Magnetizing force modeled and numerically solved for natural convection of air in a cubic enclosure: effect of the direction of the magnetic field, Int. J. Heat Mass Transfer 45 (2002) 267–277.
[5] M. Kaneda, T. Tagawa, H. Ozoe, Convection induced by a cups-shaped magnetic field for air in a cube heated from above and cooled from below, J. Heat Transfer 124 (2002) 17–25.
[6] S. Maki, T. Tagawa, H. Ozoe, Enhanced convection or quasi-conduction states measured in a super-conducting magnet for air in a vertical cylindrical enclosure heated from below and cooled from above in a gravity filed, J. Heat Transfer 124 (2002) 667–673.
[7] T. Tagawa, H. Ozoe, K. Sassa, S. Asai, Convective and diffusive phenomena of air in a vertical cylinder under a strong magnetic field, Numer. Heat Mass Transfer 41 (2002) 383–395.
[8] T. Tagawa, A. Ujihara, H. Ozoe, Numerical computation for Rayleigh–Bernard convection of water in a magnetic field, Int. J. Heat Mass Transfer 46 (2003) 4097–4104.
[9] R. Shigemitsu, T. Tagawa, H. Ozoe, Numerical computational for natural convection of air in a cubic enclosure under combination of magnetizing and gravitational forces, Numer. Heat Transfer 43 (2003) 449–463.
[10] C.H. Lee, S.S. Lu, T. Tagawa, H. Ozoe, J.M. Hyun, Numerical analysis of magnetic effect on human breathing, JSME Int. J. 46 (2003) 572–582.
[11] S. Patankar, Numerical Heat Transfer and Fluid Flow, McGraw-Hill, New York, 1980.
[12] T. Hayase, J.A.C. Humphrey, R. Grief, A consistently formulated QUICK scheme for fast and stable convergence using finite-volume iterative calculation procedures, J. Comput. Phys. 98 (1992) 108–118.
[13] J.P. Van Doorman, G.H. Raithby, Enhancements of the SIMPLE method for predicting incompressible fluid flows, Numer. Heat Transfer 7 (1984) 147–163.
[14] J. Patterson, J. Inberger, Unsteady natural convection in a rectangular cavity, J. Fluid Mech. 100 (1980) 65–86.
[15] H.S. Kwak, J.M. Hyun, Natural convection in an enclosure having a vertical sidewall with time-varying temperature, J. Fluid Mech. 329 (1996) 65–88.
[16] H.S. Kwak, K. Kuwahara, J.M. Hyun, Convective cool-down of a contained fluid through its maximum density temperature, Int. J. Heat Mass Transfer 41 (1998) 323–333.
[17] W. Lin, S.W. Armfield, Natural convection cooling of rectangular and cylindrical containers, Int. J. Heat Mass Transfer 22 (2001) 72–81.